IOP Publishing Journal of Physics D: Applied Physics
J. Phys. D: Appl. Phys. **48** (2015) 035106 (7pp) doi:10.1088/0022-3727/48/3/035106

Fundamental insights into the threshold characteristics of organic field-effect transistors

Sungyeop Jung, Chang-Hyun Kim, Yvan Bonnassieux and Gilles Horowitz

LPICM, École Polytechnique, CNRS, 91128 Palaiseau, France

E-mail: sungyeop.jung@polytechnique.edu

Received 9 October 2014, revised 17 November 2014
Accepted for publication 19 November 2014
Published 5 January 2015

Abstract

We physically model the threshold characteristics of organic field-effect transistors (OFETs) using a two-dimensional finite-element method. The transfer characteristics are simulated for staggered OFETs with various electronic structures. A reliable method to extract a structure-unique threshold voltage is presented based on the second-derivative method. By changing the hole injection barrier height in such a manner that the flat-band voltage, defined from the difference of Fermi levels of gate and source electrode, is kept constant, we demonstrate a direct impact of the hole injection barrier height on the threshold voltage. Simulated charge carrier distribution shows the two-dimensional nature of channel creation process and physical insights into the threshold characteristics of OFETs.

Keywords: organic field-effect transistors (OFETs), numerical simulation, threshold characteristics

(Some figures may appear in colour only in the online journal)

1. Introduction

Organic field-effect transistors (OFET), which were first demonstrated by Tsumura *et al* in 1986 [1], utilize organic semiconductors in place of conventional inorganic semiconductors. The device performance of OFETs has significantly improved by virtue of a better understanding of materials and fabrication processes [2]. Thanks to the improved device performance, system-level applications based on OFETs are currently sought for RF-ID tags [3–5], display backplanes [6, 7], and sensors [8].

In the early stage, physical modelling of organic semiconductors used in OFETs at a material level were of primary interest. It allowed a profound understanding of the electronic structure and the related charge carrier transport and injection processes in organic semiconductors [9, 10]. However, at a device level, it is pointed out that considerable work remains to be done to model the device physics of OFETs because the classical models, which fit well into conventional silicon based metal-oxide-semiconductor filed-effect transistors (MOSFETs), often fail to describe the behaviour of OFETs [11].

The primary benefit of physical modelling of OFETs is to improve the device performance further. In addition, results of physical modelling can be used to improve the accuracy of compact models, which consist of simple mathematical descriptions of device behaviour needed for the simulation of integrated OFET circuits [12, 13]. The rigorousness of compact modelling strongly relies on the input parameters such as the charge carrier mobility μ, contact resistance R_c, and threshold voltage V_T, which have usually been considered as constant fitting parameters [12–15]. Among them, V_T is particularly important for OFETs because of the following reasons.

Firstly, there is a lack of analytical model for V_T in OFETs. Because OFETs operate in the accumulation regime, they cannot borrow the definition of V_T from conventional MOSFETs, which operates in inversion regime as the voltage needed to create minority charge carriers to an amount equal to that of the majority carrier [11]. This accounts for the lack of an automatic extraction functionality for V_T of OFETs in most device simulators [16]. Secondly, V_T must be controllable to realize circuit-level applications. In circuit-level applications,

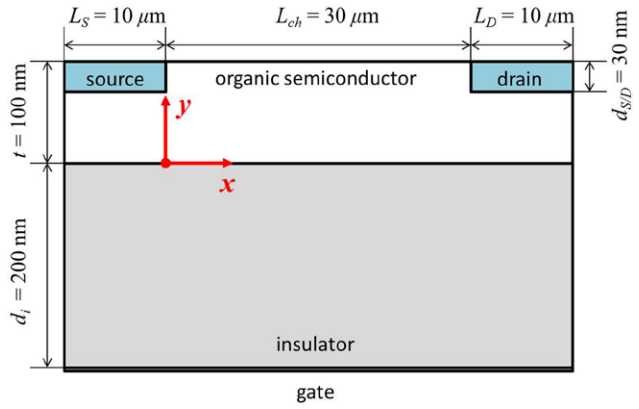

Figure 1. Device structure of the OFET which is used in the study, having a BG/TC configuration with geometrical parameters designated in the diagram. Red arrows represent conventional reference axes.

it is possible to compensate spatial deviations of V_T with the knowledge of V_T. In addition, this allows us to achieve a low voltage operation. Thirdly, V_T is highly correlated to other key parameters. For example, V_T is used to describe channel resistance $R_{ch} = 1/\{\mu\, C_i(V_G - V_T)\}$ in the extraction of contact resistance R_c by transmission-line method. In addition, other parameters are often expressed as a function of $V_G - V_T$.

In OFETs, V_T is defined as the voltage at which accumulation of charge starts [11]. For device evaluation and characterisation, V_T is estimated by parameter extraction methods from simulated or experimentally obtained transfer characteristics $I_D(V_G)$. One of the authors applied a second derivative method to OFETs for a reliable extraction of V_T, which can exclude the effect of drain voltage V_D on V_T [17]. However, the correlation between the extracted value of V_T with the definition of V_T has not yet been clearly demonstrated.

In this paper, a systematic study on physical modelling of organic field-effect transistors (OFETs) is performed based on a two-dimensional (2D) finite-element method (FEM). Through the systematic numerical simulation based on FEM, we try to clarify the contributions of device parameters on V_T, which is necessary to formulate a more rigorous analytical model.

2. Simulation methods

A numerical modelling is conducted by using ATLAS simulator (SILVACO) which self-consistently resolves the drift-diffusion current equation and the Poisson's equation. With FEM-based ATLAS simulator, not only the transfer characteristics $I_D(V_G)$ of OFETs but also physical parameters, such as electric potential and electron and hole concentration, can be calculated at each mesh, which are small domains constructing the device. Figure 1 shows the simulated p-type OFET structure with a bottom-gate/top-contact (BG/TC) configuration. The physical dimensions of the device and the point of origin on a 2D plane are not changed throughout the simulation.

The physical and electrical properties of the materials used in the simulation are summarized in table 1. The

Table 1. Physical and electrical parameters used in the simulation.

Categories	Parameters	Values
Physical dimensions	Source/Drain length ($L_{S/D}$)	10 μm
	Channel length (L_{ch})	30 μm
	Channel width (W_{ch})	1000 μm
	Source/Drain thickness ($d_{S/D}$)	30 nm
	Semiconductor thickness (t)	100 nm
	Insulator thickness (d_i)	200 nm
Gate electrode	Work function (W_G)	4.3 eV
Source/Drain electrodes	Work function ($W_{S/D}$)	4.9 eV
Insulator	Dielectric constant (k_i)	3
Organic semiconductor	HOMO effective DOS (N_v)	10^{20} cm^{-3}
	Dielectric constant (k)	3
	Doping concentration (N_A)	0 cm^{-3}
	Band gap (E_g)	2.4 eV
	HOMO level	5.2 eV
	Hole mobility (μ)	0.5 cm^2 V^{-1} s^{-1}
	Defect density of states (N_T)	0 cm^{-2} eV^{-1}

electronic structure of the simulated p-type OFET is determined by the work functions W of the metal electrodes, and the highest-occupied molecular orbital (HOMO) level and band gap E_g of the organic semiconductor. It is particularly important to note that we assume a zero-doped and defect-free organic semiconductor. Organic semiconductors are usually used without intentional doping for OFETs; we showed that the unintentional dopants incorporated with a moderate concentration (roughly up to 10^{14} cm^{-3}) do not significantly affect the device characteristics as has been shown for organic diodes [18], organic metal-semiconductor field-effect transistors (OMESFETs) [19] and OFETs (see the supporting material). Moreover, the defect-free case is assumed in order to study V_T in relation to the electronic structure of the OFET, excluding any role of defects which have been reported to have a significant effect on V_T [17, 20–23]. The defect (or trap) states created in the forbidden gap accommodate and immobilize charge carriers, which modify the electronic structure and the charge carrier concentration in OFETs. Because the defect-free case is hard to achieve experimentally, it is a distinctive merit of simulation to be able to neglect the effect of traps.

Threshold in OFETs occurs at a low voltage. In addition, it has been reported that the injection property at the metal-organic semiconductor junction is one of the most significant aspects that governs the device operation at low voltages [18]. In this context, we varied the injection barrier height E_b at source (and drain) by varying the ionization energy (IE) of the organic semiconductor while keeping E_g constant to study the effect of charge carrier injection on V_T. Because we did not directly change the Fermi level of the source and drain electrodes, the flat-band potential V_{FB}, which is defined as

the Fermi level difference between gate and source (or drain) electrodes, was unaffected by the modification of E_b.

3. Results and discussion

3.1. Threshold voltage extraction and the 'structure-unique' threshold voltage

A rigorous analytical model for V_T of OFETs is still lacking. Therefore, V_T was extracted from simulated transfer characteristics $I_D(V_G)$ in order to be used for device analysis. The linear-regime drain current $I_D(V_G)$ of a p-type OFET is expressed as,

$$I_D(V_G) = -\frac{W}{L}\mu C_i\left\{(V_G - V_T)V_D - \frac{V_D^2}{2}\right\}, \quad (1)$$

where W and L are the channel width and length respectively, μ is the field-effect mobility, C_i the capacitance of the insulator, and V_D the drain voltage. Extraction methods used for conventional MOSFETs such as the constant current method [24], linear extraction method (LEM) [24, 25], and second derivative method (SDM) [26] are also applicable to OFETs. However, it has been often overlooked that V_T should be a structure-unique value. By the term 'structure-unique', we emphasize the dependence of V_T only on the electronic structure of the device without the dependence on the bias condition and the extraction method.

A reliable extraction method should be able to determine V_T as a single constant. In LEM, V_T is estimated at the intercept of the voltage axis with the $I_D(V_G)$ line. The approximation is made at the voltage point corresponding to the maximum slope of $I_D(V_G)$ curve [27]. However, the maximum slope point is uncertain when the $I_D(V_G)$ curve deviates from an ideal straight line. For example, if the $I_D(V_G)$ curve is bended downward over V_T (concave down with positive slope) due to mobility degradation and/or the existence of a source and drain contact resistance R_C, the point of maximum slope becomes dependent on the mobility degradation and R_C. Similarly, if the $I_D(V_G)$ curve is bended upward (concave up with positive slope), the point of the maximum slope does not even exist. Although a range of V_G that allows the best possible linear fit, can be arbitrarily chosen [28], the extracted value of V_T become dependent on the choice of bias range. On the other hand, in SDM, V_T is defined as the V_G at which the second-order derivative of $I_D(V_G)$ curve is maximum. It corresponds to V_G where the change of conductivity is the fastest, which is not affected by R_C. In most cases, it is possible to specify V_T from the distinctive peak of the second-derivative $\partial^2 I_D(V_G)/\partial V_G^2$.

Secondly, a reliable extraction method should exclude the dependancy of V_T on V_D. Instead of impetuously neglecting the second-order term $V_D^2/2$ in equation (1) for linear regime approximation, it is more desirable to collect the common V_D factor,

$$I_D(V_G) = -\frac{W}{L}\mu C_i\left\{V_G - \left(V_T + \frac{V_D}{2}\right)\right\}V_D, \quad (2)$$

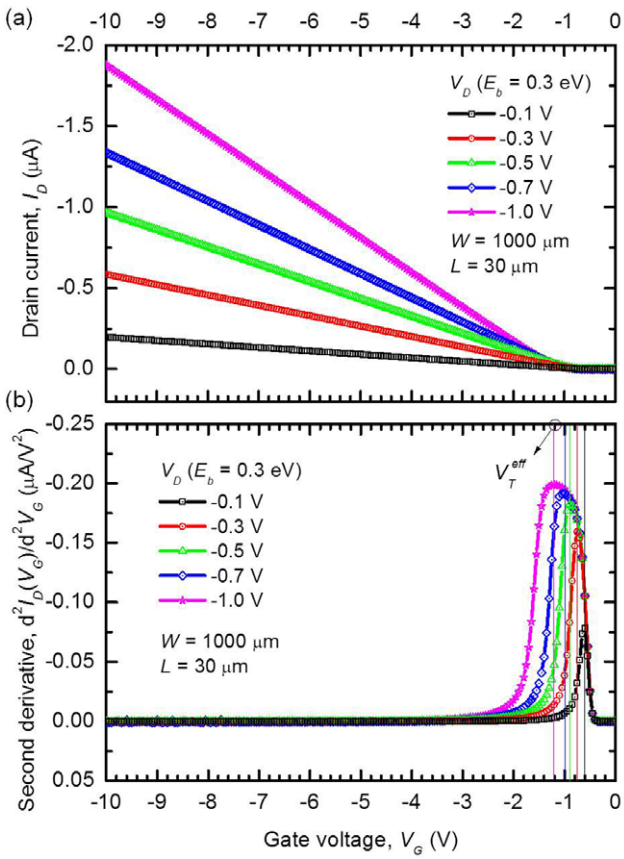

Figure 2. (*a*) Simulated linear-regime transfer characteristics $I_D(V_G)$ of OFETs with drain voltage V_D as a parameter (V_D = − 0.1, −0.3, −0.5, −0.7 and −1.0 V). (*b*) Second derivatives of the simulated $I_D(V_G)$ which show the effective threshold voltage V_T^{eff} at each peak.

where $V_T + V_D/2$ is defined as the effective threshold voltage V_T^{eff}. Then, V_D independent V_T can be determined as the y-intercept of an extrapolation line of V_T^{eff} with respect to V_D, which can be obtained from different $I_D(V_G)$ curves at different V_D.

In figure 2, numerically simulated linear-regime $I_D(V_G)$ and $\partial^2 I_D(V_G)/\partial V_G^2$ are shown for a BG/TC OFET biased at V_D = − 0.1, −0.3, −0.5, −0.7, and −1.0 V, while the injection barrier height E_b is kept unchanged at 0.3 eV. It is observed that a slight upward-bending and a leftward-shift of the simulated $I_D(V_G)$ occur as the drain voltage increases (figure 2(*a*)). This reflects the depedence of V_T^{eff} on V_D which is demonstrated by the leftward-shifted peak of $\partial^2 I_D(V_G)/\partial V_G^2$ as shown in figure 2(*b*). In addition, the voltages can be specified without any ambiguity by referring to the peaks of $\partial^2 I_D(V_G)/\partial V_G^2$. The V_T^{eff} extracted from figure 2(*b*) is plotted as a function of V_D (see figure 4). At the y-intercept of the extrapolated linear line for V_T^{eff}, the structure-unique V_T is determined as 0.5 V for the case of E_b = 0.3 eV.

In many reports, V_T is regarded as equivalent to the flat-band voltage V_{FB} when no dipole moment and trapped charges exist at gate/insulator and insulator/organic semiconductor interfaces [28, 29]. In the meantime, V_{FB} has been determined without clear remarks on the free carrier concentration in organic semiconductor layer at equilibrium. For OFETs

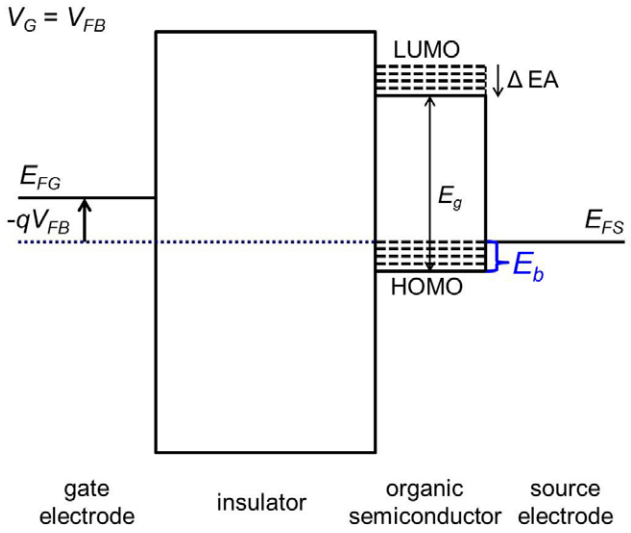

Figure 3. Energy diagram based on the metal-insulator-insulator-metal (MIIM) model for various hole injection barrier height E_b: E_b = 0.0, 0.1, 0.2, 0.3, and 0.4 eV.

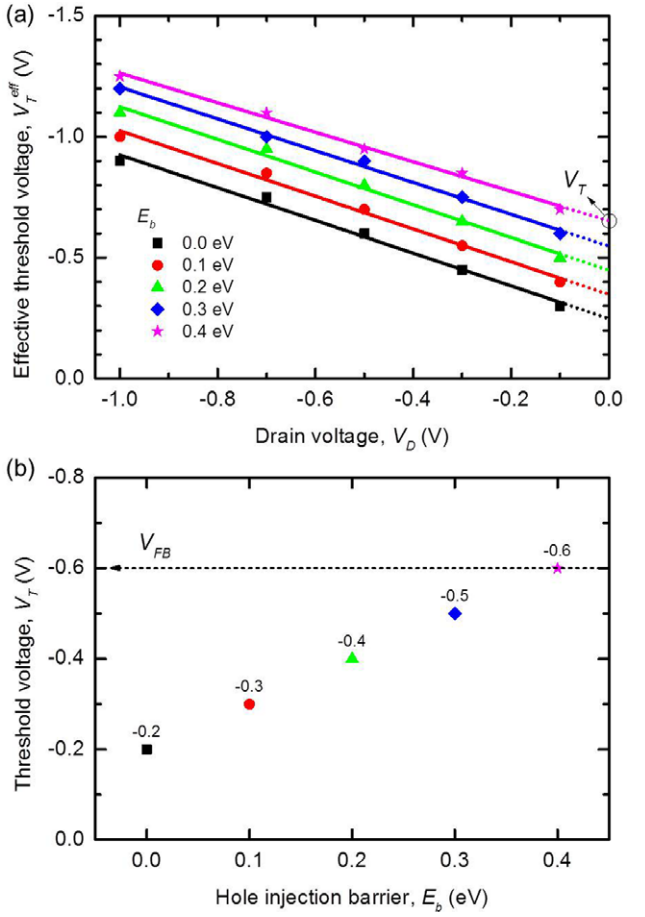

Figure 4. (*a*) Extracted values of effective threshold voltage V_T^{eff} by the second-derivative method for OFETs for various barrier heights (E_b = 0.0, 0.1, 0.2, 0.3, and 0.4 eV.) plotted with respect to drain voltage V_D. (*b*) The threshold voltage V_T as a function of the hole injection barrier height E_b. The flat band voltage V_{FB} is indicated for comparison. Note that $V_T \neq V_{FB}$ for $E_b < 0.4$ eV.

using intentional doping to achieve high carrier concentration, the conventional definition for V_{FB} of the MOS structure in MOSFETs, defined from the Fermi level difference of the gate electrode and the organic semiconductor, is equally valid for OFETs. On the other hand, when organic semiconductors are not doped as in the case of this study, V_{FB} is defined in a different manner. It was well demonstrated that, for non-doped organic diodes, the depletion region extends up to the organic semiconductor/metal interface due to (i) much smaller thickness of organic layer (around 100 nm) compared to silicon wafer (around 0.7 mm) and (ii) extremely low carrier concentration (typically 10^{14} cm^{-3}) [18, 30]. This makes possible an analogy of the organic layer with an insulator in the metal-insulator-metal (MIM) model. Similarly, the electronic structure of OFETs is often seen as the metal-insulator-insulator-metal (MIIM) structure comprising the source electrode [31]. Accordingly, V_{FB} is defined from the Fermi level difference of the gate and source electrode, which will be used as the definition for V_{FB} herein.

Based on the MIIM model, the energy diagram of an OFET at $V_{FB} = V_{FB}$ can be schematically drawn, as in figure 3. If we assume that the MIIM model is applicable at all E_b, V_T should be equal to V_{FB} and should be invariant with respect to E_b because E_b is varied while keeping the Fermi levels of gate and source constant. However, as shown in figure 4, a direct impact of E_b on the structure-unique V_T is indeed observed. Figure 4(*b*) shows that V_T is equal to V_{FB}, and thus the MIIM model is strictly valid only for an electronic structure, E_b = 0.4 eV. However, the MIIM model cannot be adopted to estimate V_T when $E_b < 0.4$ eV even if no interface charges and defects are considered. This demonstrates the importance of injection properties at organic semiconductor/source interface in defining the threshold behaviour in OFETs. When E_b gets higher than 0.4 eV, the drain current is strongly reduced and the transfer curve deviates from a straight line, thus hindering any reliable estimation of the threshold voltage. We also note that such a high barrier height is not realistic for any practical application of the transistor [32].

3.2. Physical meaning of the threshold voltage

In the previous section, we demonstrated that the structure-unique threshold voltage V_T is not equal to the flat-band voltage V_{FB} determined from the MIIM model when the hole injection barrier height E_b is smaller than 0.4 eV. This result accounts not only for the modified injection properties, but also for the fact that the OFET is a two-dimensional (2D) device as opposed to the one-dimensional (1D) organic diodes. In this respect, the threshold behaviour needs to be understood not only across the channel, which corresponds to the MIIM structure, but also along the channel.

Figure 5 shows the numerically simulated hole concentration p_{xy} in the organic layer of an OFET with a hole injection barrier height of 0.3 eV at different gate bias: (*a*) for V_G = 0 V, (*b*) for $V_G = V_{FB} = -0.6$ V, and (*c*) for $V_G = -5$ V. At equilibrium, V_G = 0 V (see figure 5(*a*)), p_{xy} greatly varies inside the organic layer. Near the center of the channel x = 15 μm, p_{xy} shows an extremely low value (around 10^5 cm^{-3}).

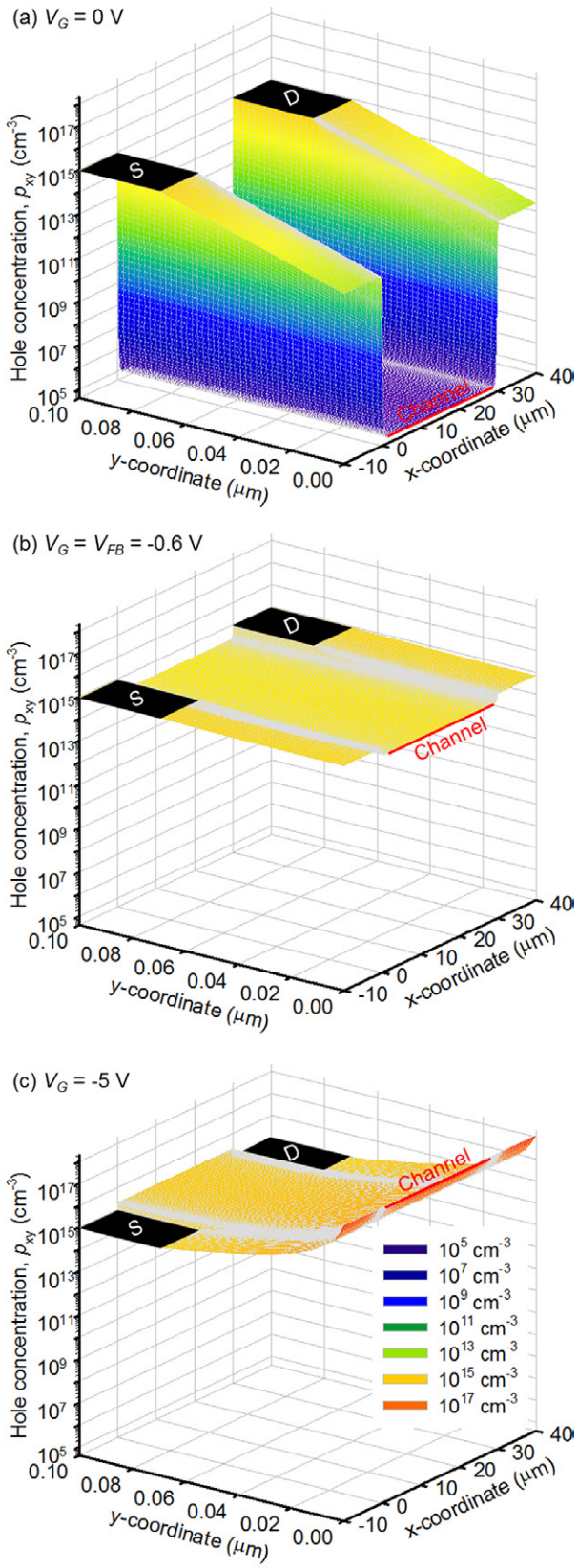

Figure 5. Simulated hole concentration in the OFET at different bias conditions: (*a*) V_G = 0 V, (*b*) V_G = V_{FB} = – 0.6 V and (*c*) V_G = – 5 V. For each condition, V_D = 0 V and E_b = 0.3 eV. The y-coordinate represents the distance from insulator/organic semiconductor interface, while the *x*-axis is parallel to the interface. The center of channel and the center of source electrode corresponds to *x* = 15 and *x* = – 5 μm.

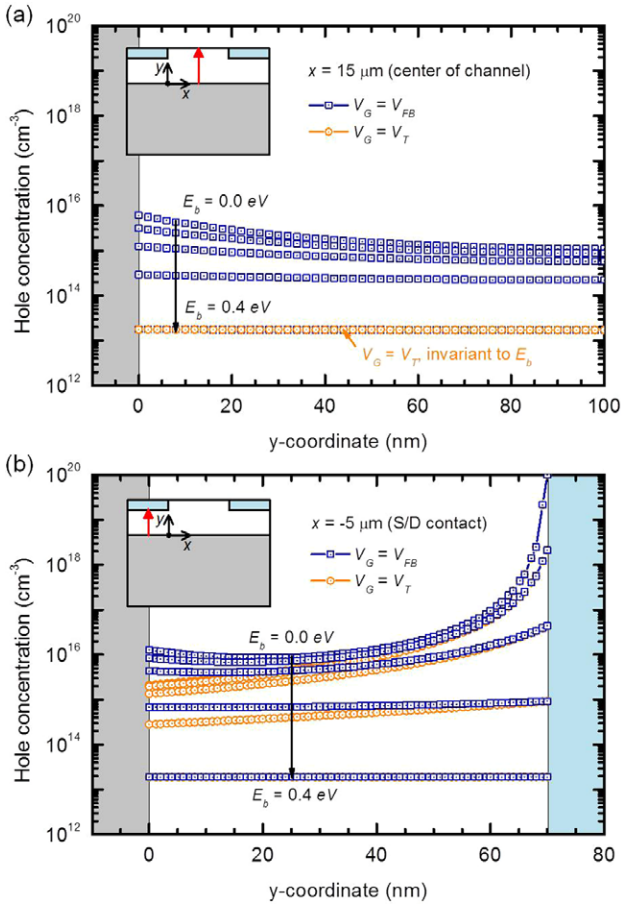

Figure 6. Simulated hole concentration across the channel (along *y*-axis) sectioned (*a*) at the center of channel (*x* = 15 μm) and (*b*) at the center of source electrode (*x* = – 5 μm) for two bias conditions: V_G = V_{FB} = – 0.6 V and V_G = V_T. The hole injection barrier height E_b is varied from 0.0 to 0.4 eV. Accordingly, the value of threshold voltage V_T varies following the electronic structure of each OFET (figure 4(*b*)).

In contrast, p_{xy} along *x* = – 5 and *x* = 35 μm, which corresponds to the MIIM structure, takes 7–10 order of magnitude larger value because of the effect of source and drain electrode. At V_G = V_{FB} = – 0.6 V, injected holes are filling the center of the channel, and the spatial distribution of p_{xy} is nearly, but not perfectly, uniform in the organic layer. At V_G = – 5 V, p_{xy} is several orders of magnitude higher at the insulator/organic semiconductor interface than in the bulk, due to accumulation by a large negative bias applied at gate electrode, thus reaching to the creation of the conducting channel. The spatial distribution of p_{xy} greatly changes along the *x*-axis, especially for an OFET in sub-threshold regime, so that a systematic analysis is desirable to compare the spatial distribution of p_{xy} at two characteristic lines along *y*-axis, that is the center of channel (*x* = 15 μm) and at the center of the source electrode (*x* = – 5 μm).

Figure 6(*a*) shows the spatial distribution of p_{xy} at the center of the channel (*x* = 15 μm) across the channel (along *y*-axis) of OFETs with various electronic structures for two gate bias conditions: V_G = V_{FB} = – 0.6 V (squares in navy), and V_G = V_T (circles in orange). The hole injection barrier height E_b is varied as 0.0, 0.1, 0.2, 0.3, and 0.4 eV, where the

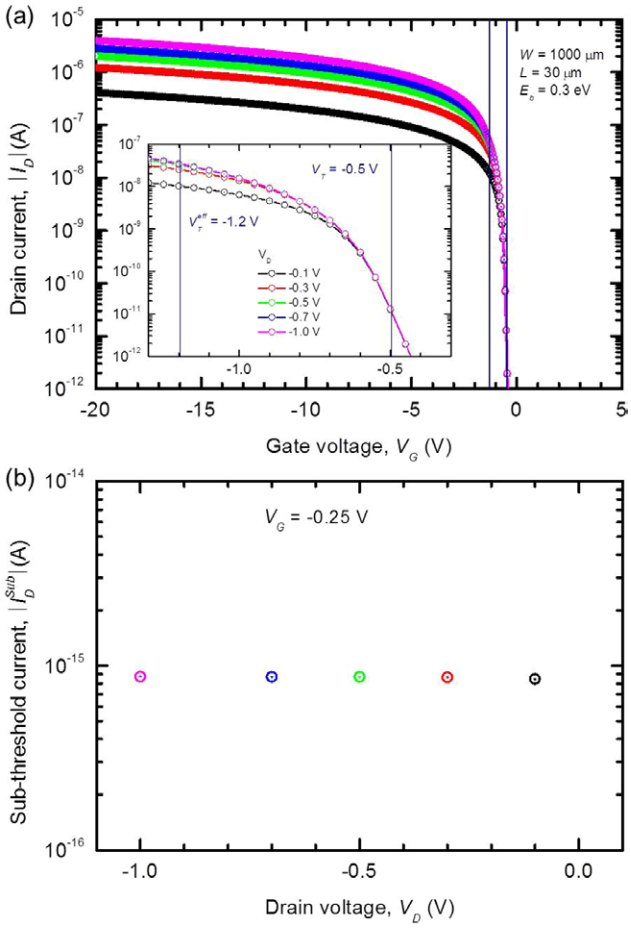

Figure 7. (*a*) Simulated linear-regime transfer characteristics $I_D(V_G)$ of OFETs in log-scale with drain voltage V_D as a parameter (V_D = – 0.1, –0.3, –0.5, –0.7 and –1.0 V). (Inset) Close-up of $I_D(V_G)$ with V_T = – 0.5 V and V_T^{eff} = –1.2 V as a guide to an eye. (*b*) Sub-threshold current read from V_G = – 0.25 V for various drain voltage V_D. Hole injection barrier height E_b is 0.3 eV.

structure-unique threshold voltage V_T changes correspondingly as shown in figure 4(*b*). When the flat-band voltage V_{FB} based on the MIIM model –0.6 V is applied, the spatial distribution of p_{xy} across the channel is flat only for the case of E_b = 0.4 eV, where V_{FB} happens to be equal to V_T. For other barrier heights, E_b = 0.0, 0.1, 0.2, and 0.3 eV, the OFETs are already turned on when V_{FB} is applied because V_{FB} is bigger than V_T. On the other hand, when $V_G = V_T$, the spatial distribution of p_{xy} across the channel is constant for every electronic structure, and hence the potential. This demonstrates that the threshold voltage can be defined as the voltage at which charge starts to accumulate at the insulator/organic semiconductor interface at the center of the channel. In addition, this physical meaning of threshold voltage is a universal description which is valid for every electronic structure, and well represented by the structure-unique V_T other than V_{FB}.

Figure 6(*b*) shows the spatial distribution of p_{xy} at the center of source electrode (x = – 5 μm) across the channel (along y-axis), which corresponds to MIIM structure, of OFETs having various electronic structures for two gate bias conditions: for $V_G = V_{FB}$ = – 0.6 V (squares in navy), and $V_G = V_T$ (circles in orange). The hole concentration at the organic semiconductor/source interface is determined by

$$p_s = N_V \exp\left(-\frac{E_b}{kT}\right), \tag{3}$$

where N_V denotes the HOMO effective density-of-states (DOS), E_b hole injection barrier height, k Boltzmann constant, and T temperature (300 K). As the injection of holes becomes more favoured thanks to lowered E_b, the concentration of holes injected from the organic semiconductor/source interface increases. As a consequence, potential in organic layer deviates from a perfectly linear line and shows significant bending near organic semiconductor/source interface when E_b < 0.4 eV. For this reason, it is hard to define either V_{FB} or V_T at the center of source or drain electrode.

3.3. Sub-threshold current

A reliable extraction method of V_T based on the SDM is demonstrated to compute a structure-unique V_T which excludes the effect of drain voltage V_D and inherent ambiguity from some extraction methods, and which is coherent to the physical meaning of threshold voltage. In this section, sub-threshold characteristics are studied in reference to structure-unique V_T.

Figure 7(*a*) shows the simulated transfer characteristics $I_D(V_G)$ of OFETs in semi-log plot. The drain voltage V_D is varied as –0.1, –0.3, –0.5, –0.7 and –1.0 V, and hole injection barrier height E_b is set to 0.3 eV, where the structure-unique V_T is –0.5 V and effective-threshold voltage V_T^{eff} is –1.2 V for V_D = – 1.0 V (see figure 4). With the help of two guide lines for V_T and V_T^{eff} in figure 7, it is shown that the current at gate voltage V_G larger than V_T = – 0.5 V shows V_D dependence, which demonstrates that the current is realized by both diffusion and drift of charge carriers. On the other hand, for V_G smaller than V_T = – 0.5 V, it is shown that the current does not depend on V_D. Figure 7(*b*) shows $I_D(V_G)$ read at V_G = – 0.25 V as an example. The variation of V_D does not affect $I_D(V_G)$, which is a characteristic of conduction solely mediated by diffusion of carriers. This proves that the sub-threshold region of OFETs can be successfully defined by the structure-unique V_T obtained from aforementioned method.

4. Conclusion

We have investigated the threshold behaviour of OFETs. The proposed extraction method for threshold voltage V_T based on second-derivative method (SDM) enabled determination of a structure-unique V_T excluding the effects of drain voltage V_D. By the structure-unique V_T, we defined the threshold voltage as the voltage where accumulation starts at the center of channel, which is shown to be universally valid for all electronic structures. At the same time, the flat-band voltage V_{FB} adopted form the metal-insulator-insulator-metal model was shown to have limited applicability for OFETs with hole injection barrier height (E_b = 0.4) in the definition of V_T. In the gate voltage range smaller than the structure-unique V_T,

the sub-threshold region of OFETs could be successfully determined, where only the diffusion of carriers contributes to drain current.

Acknowledgments

The work of S Jung was supported by the Vice Presidency for External Relations (DRI) of the Ecole Polytechnique through a PhD fellowship.

References

[1] Tsumura A, Koezuka H and Ando T 1986 *Appl. Phys. Lett.* **49** 1201
[2] Klauk H 2010 *Chem. Soc. Rev.* **39** 2643
[3] Drury C J, Mutsaers C M J, Hart C M, Matters M and de Leeuw D M 1998 *Appl. Phys. Lett.* **73** 108
[4] Baude P F, Ender D A, Haase M A, Kelley T W, Muyres D V and Theiss S D 2003 *Appl. Phys. Lett.* **82** 3964
[5] Cantatore E, Geuns T C T, Gelinck G H, van Veenendaal E, Gruijthuijsen A F A, Schrijnemakers L, Drews S and de Leeuw D M *IEEE J. Solid-State Circuits* **42** 84–92
[6] Sirringhaus H, Tessler H and Friend R H 1998 *Science* **280** 1741–4
[7] Dodabalapur A, Bao Z, Makhija A, Laquindanum J G, Raju V R, Feng Y, Katz H E and Rogers J 1998 *Appl. Phys. Lett.* **73** 142
[8] Angione M D *et al* 2011 *Mater. Today* **14** 424–33
[9] Metzger R M 2012 *Unimolecular and supramolecular electronics I* Charge transport in organic semiconductors vol 312 (Berlin Springer)
[10] Burin A L and Ratner M A 2003 *J. Polym. Sci. B: Polym. Phys.* **41** 2601–21
[11] Horowitz G, Hajlaoui R, Bouchriha H, Bourguiga R and Hajlaoui M 1998 *Adv. Mater.* **10** 923
[12] Estrada M, Cerdeira A, Puigdollers J, Reséndiz L, Pallares J, Marsal L F, Voz C and Iñiguez B 2005 *Solid-State Electron.* **49** 1009–16
[13] Iñiguez B, Picos R, Veksler D, Koudymov A, Shur M S, Ytterdal T and Jackson W 2008 *Solid-State Electron.* **52** 400–5
[14] Kim C H, Castro-Carranza A, Estrada M, Cerdeira A, Bonnassieux Y, Horowitz G and Iñiguez B 2013 *IEEE Trans. Electron Devices* **60** 1136–41
[15] Street R A and Salleo A 2002 *Appl. Phys. Lett.* **81** 2887
[16] SILVACO 2014 *DeckBuild User's Manual* (Santa Clara, CA: SILVACO International)
[17] Braga D and Horowitz G 2009 *Appl. Phys.* A **95** 193–201
[18] Kim C H, Yaghmazadeh O, Bonnassieux Y and Horowitz G 2011 *J. Appl. Phys.* **110** 093722
[19] Kim C H, Tondelier D, Geffroy B, Bonnassieux Y and Horowitz G 2011 *Eur. Phys. J. Appl. Phys.* **56** 34105
[20] Noh Y Y, Kim D Y, Yoshida Y, Yase K, Jung B J, Lim E and Shim H K 2005 *Appl. Phys. Lett.* **86** 043501
[21] Pernstich K P, Haas S, Oberhoff D, Goldmann C, Gundlach D J, Batlogg B, Rashid A N and Schitter G 2004 *J. Appl. Phys.* **96** 6431
[22] Sangeeth C S S, Stadler P, Schaur S, Sariciftci N S and Menon R 2010 *J. Appl. Phys.* **108** 113703
[23] Podzorov V, Menard E, Borissov A, Kiryukhin V, Rogers J A and Gershenson M E 2004 *Phys. Rev. Lett.* **93** 086602
[24] Schroeder D 1998 *Semiconductor Material and Device Characterization* 2nd edn (New York: Wiley)
[25] Liou J J, Ortiz-Conde A and García Sánchez F J 1998 *Analysis and Design of MOSFETs: Modeling, Simulation and Parameter Extraction* (Boston, MA: Kluwer Academic)
[26] Wong H S, White M H, Krutsick T J and Booth R V 1987 *Solid-State Electron.* **30** 953–68
[27] Ortiz-Conde A, García Sánchez F J, Liou J J, Cerdeira A, Estrada M and Yue Y 2002 *Microelectron. Reliab.* **42** 583–96
[28] Wang A, Kymissis I, Bulović V and Akinwande A I 2006 *Appp. Phys. Lett.* **89** 112109
[29] Tal O, Rosenwaks Y, Roichman Y, Preezant Y, Tessler N, Chan C K and Kahn A 2006 *Appl. Phys. Lett.* **88** 043509
[30] Kim C H, Bonnassieux Y and Horowitz G 2014 *IEEE Trans. Electron Devices* **61** 278–87
[31] Ou-Yang W, Weis M, Taguchi D, Chen X, Manaka T and Iwamoto M 2010 *J. Appl. Phys.* **107** 124506
[32] Brondijk J J, Torricelli F, Smits E C P, Blom P W M and de Leeuw D M 2012 *Org. Electron.* **13** 1526–31